IOPscience iopscience.iop.org

Home Search Collections Journals About Contact us My IOPscience

The electronic configuration of Fe in β–$FeSi_2$

This article has been downloaded from IOPscience. Please scroll down to see the full text article.

1997 J. Phys.: Condens. Matter 9 1619

(http://iopscience.iop.org/0953-8984/9/7/023)

View the table of contents for this issue, or go to the journal homepage for more

Download details:
IP Address: 171.66.16.207
The article was downloaded on 14/05/2010 at 08:09

Please note that terms and conditions apply.

J. Phys.: Condens. Matter **9** (1997) 1619–1630. Printed in the UK PII: S0953-8984(97)78188-8

The electronic configuration of Fe in β-$FeSi_2$

M Fanciulli†, C Rosenblad†, G Weyer†, A Svane†, N E Christensen†, H von Känel‡ and C O Rodriguez§

† Institute of Physics and Astronomy, University of Aarhus, DK-8000 Aarhus C, Denmark
‡ Laboratory for Solid State Physics, ETH-Zürich, CH-8093 Zürich, Switzerland
§ Instituto di Fisica de Liquidos y Sistema Biologica, Grupo de Fisica del Solido, CC 565, La Plata, Argentina

Received 27 September 1996

Abstract. The experimental results obtained by ^{57}Fe conversion electron Mössbauer spectroscopy on the electronic configuration of Fe in β-$FeSi_2$ are discussed in the light of *ab initio* full-potential linear muffin-tin orbital calculations of the isomer shift δ, quadrupole splitting Δ and asymmetry parameter η for the two Fe sites.

1. Introduction

The bulk stable semiconducting disilicide β-$FeSi_2$ has attracted increasing interest during the last few years due to its potential optoelectronic applications, related to the direct gap of $\approx$0.85 eV [1–4], when it is integrated into the well developed Si technology. However, theoretical [5, 6] and experimental evidence [7] of a slightly lower indirect transition casts doubts on the applications of this compound for light-emitting devices. The wide range of optical band gaps reported for this material and the controversial results on the direct or indirect nature of the transition seems to be related to a high density of defects producing band tails which, by merging with the parent band, alter the intrinsic band structure [8].

At the Fe/Si composition ratio of 1:2 two bulk phases are known of [9]. The α-$FeSi_2$ phase, stable at temperatures between 967 °C and 1223 °C, is metallic and has a tetragonal lattice. At temperatures lower than 967 °C the semiconducting β-$FeSi_2$ phase is formed. Due to a Jahn–Teller-like instability of the fluorite phase [3] β-$FeSi_2$ crystallizes in a base-centred orthorhombic lattice with $a = 0.7791$ nm, $b = 0.7833$ nm and $c = 0.9863$ nm, belonging to the space group $Cmca$ (D_{2h}^{18}) [10]. The primitive cell contains 24 atoms and the 8 Fe atoms are grouped in two different Fe sites, each surrounded by a distorted cube of Si atoms, but with different Fe–Si distances [10]: Fe_I has Fe–Si = 0.234–0.239 nm, while Fe_{II} has Fe–Si = 0.233–0.244 nm. The epitaxial growth of β-$FeSi_2$ on Si(100) results in the heteroepitaxial relationship β-$FeSi_2$(001)/Si(001). Two types of lattice matching can be obtained: (A) β-$FeSi_2$[100]$\|$Si$\langle$110$\rangle$ and (B) β-$FeSi_2$[100]$\|$Si$\langle$100$\rangle$ [11]. This results in two types of grain rotated by $\pi/4$ around the normal to the Si substrate. Each type of grain can furthermore be rotated by $\pi/2$ around the normal to the Si substrate [11, 12].

Earlier Mössbauer investigations [13, 14] on single-crystalline and polycrystalline samples gave puzzling results. The Mössbauer spectrum, fitted with four lines with isomer shifts (δ relative to (the isomer shift of) α-Fe at room temperature) of $\delta_1 = -0.187(4)$, $\delta_2 = -0.067(4)$, $\delta_3 = +0.248(4)$ and $\delta_4 = +0.338(4)$ (reference [16]), presented the problem of the determination of the correct coupling between these lines in order to identify the two

0953-8984/97/071619+12$19.50 © 1997 IOP Publishing Ltd

quadrupole doublets related to the two Fe sites of the orthorhombic structure. The ambiguity has been addressed by Wandji *et al* [13] who concluded, on the basis of point charge calculations for the electric field gradients (EFG) at the two sites, that the coupling between lines 1–3 and 2–4 was the correct one and obtained the following Mössbauer parameters: $\delta_{\mathrm{I}} = 0.14$, $\Delta_{\mathrm{I}} = 0.40$, $\delta_{\mathrm{II}} = 0.03$, $\Delta_{\mathrm{II}} = 0.44$. The distorted cubes of Si atoms around the Fe sites produce an EFG at the nucleus which accounts for the observed quadrupole interaction while the observed isomer shifts are determined by the average distances characterizing the two sites [13]. Similar results have been obtained by Blaauw and co-workers [14] and by Helgason and Sigfüsson [15].

Our study [16] of the electronic Fe configuration in epitaxial β-$FeSi_2$ by ^{57}Fe conversion electron Mössbauer spectroscopy (CEMS) has shown that, on the basis of the angular dependence of the line intensities, the correct coupling of the lines is 1–4 and 2–3 or 1–2 and 3–4, whereas the previously adopted coupling (1–3 and 2–4) is inconsistent with the experimental results. *Ab initio* linear muffin-tin orbital (LMTO) calculations within the atomic-sphere approximation (ASA) of the electronic density at the two sites highly favoured the coupling 1–4 and 2–3 [16]. The experiments [16] showed that the main principal axes of the electric field gradient tensors for the two Fe sites are parallel to the *c*-axis and that the EFG values along this axis are pronouncedly different and opposite in sign, whereas the total electron densities as given by the isomer shifts are similar.

In this paper we report on a detailed comparison between the experimental results and *ab initio* full-potential (FP) LMTO calculations within the local density approximation of the isomer shift and EFG [17] parameters for the two Fe sites in β-$FeSi_2$.

2. Experimental methods

β-$FeSi_2$ was grown in a commercial MBE system by stoichiometric electron-gun co-deposition of Fe and Si on n-type, not intentionally misoriented ($<0.3^\circ$) Si(001). The growth procedure consisted of several steps involving first the formation of a 10 nm thick β-$FeSi_2$ template, followed by MBE up to the final thickness at a substrate temperature of 700 °C. Details on the growth and characterization have been given elsewhere [12].

CEMS measurements have been performed at room temperature using a 50 mCi ^{57}Co in a Rh matrix source which was moved by a standard constant-acceleration drive. The isomer shifts δ are given relative to α-Fe: a positive value of δ means that the isomeric transition has a higher energy than in α-Fe. In view of the negative calibration constant [18] this also means a lower electron density than in α-Fe. The samples were incorporated as electrodes in a parallel-plate avalanche detector [19]. The detector probes a depth of about 200 nm given by the ranges of the various conversion, Auger and secondary photoelectrons emitted after the nuclear resonance absorption. This ensures negligible line broadening due to the absorber thickness while simultaneously the detector construction is optimized for both an effect-to-background ratio and electron detection efficiency close to the theoretical limits. Thus Mössbauer spectra of very high quality with an energy resolution close to the limit of twice the natural width are obtained.

3. Experimental results

The sample investigated, 750 nm thick, exhibits pure type-A orientation. However, due to rotational domains ($\pi/2$ around *c*-axes) it is not a single crystal. Rutherford backscattering measurements (RBS), performed with 2 MeV $^4He^+$ ions, give a minimum channelling yield

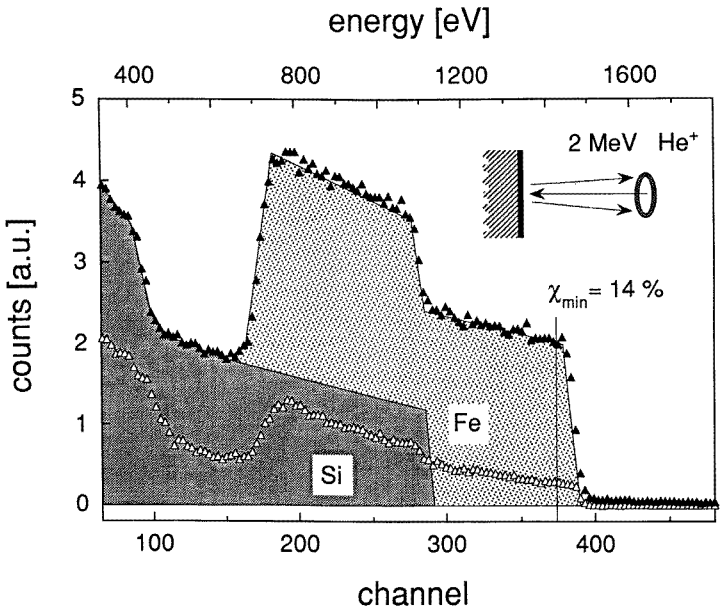

Figure 1. RBS results for the film investigated for random (filled triangles) and channelling (open triangles) conditions.

of 14% as shown in figure 1.

The CEMS spectra are shown in figure 2. In agreement with previous investigations [13, 14] we found four Lorentzian lines with isomer shifts of $\delta_1 = -0.187(4)$, $\delta_2 = -0.067(4)$, $\delta_3 = +0.248(4)$ and $\delta_4 = +0.338(4)$ [16]. The observed linewidth $\Gamma = 0.23(2)$ corresponds to the minimum experimental width indicating a good crystal quality. A narrow linewidth is of utmost importance for the determination of the angular dependence of the line intensities for lines 1 and 2 and lines 3 and 4 which are separated by isomer shift differences of only about $\Gamma/2$. The considerable overlap between these lines makes it difficult to assess the angular dependence of their intensity. The spectral quality allowed us to exploit fully the sharpening procedure described by Afanas'ev and Tsymbal [20] without visible loss of statistical accuracy [16]. From this analysis it was possible to prove that the previously accepted quadrupole couplings of lines 1–3 and 2–4 has to be discarded and that the correct coupling is between lines 1–4 and 2–3 or 1–2 and 3–4 [16]. Figure 3 shows the angular dependence of the ratio of the intensities of the higher- and lower-energy lines for the coupling 1–4 and 2–3, i.e. A_4/A_1 and A_3/A_2, as well as the ratio of the sums $(A_1+A_4)/(A_2+A_3)$. The latter ratio is seen to be close to 1, reflecting the equal population of the two different Fe lattice sites. Given this population ratio for the two sites, the constancy of the sum ratio to within 10% proves the accuracy of the spectral deconvolution in terms of overlapping lines to be about 10% and the Lamb–Mössbauer factor for the two sites to be the same and isotropic, i.e. indicates the absence of a Goldanskii–Karyagin effect [21], within the experimental accuracy. Figure 4 shows the angular dependence of the ratio of the intensities of the higher- and lower-energy lines for the coupling 1–2 and 3–4, i.e. A_2/A_1 and A_4/A_3, as well as the ratio of the sums $(A_1 + A_2)/(A_3 + A_4)$. Despite the fact that this coupling will be shown to be incompatible with theoretical results, the observation that the ratio $(A_1 + A_2)/(A_3 + A_4)$ is independent of angle provides additional

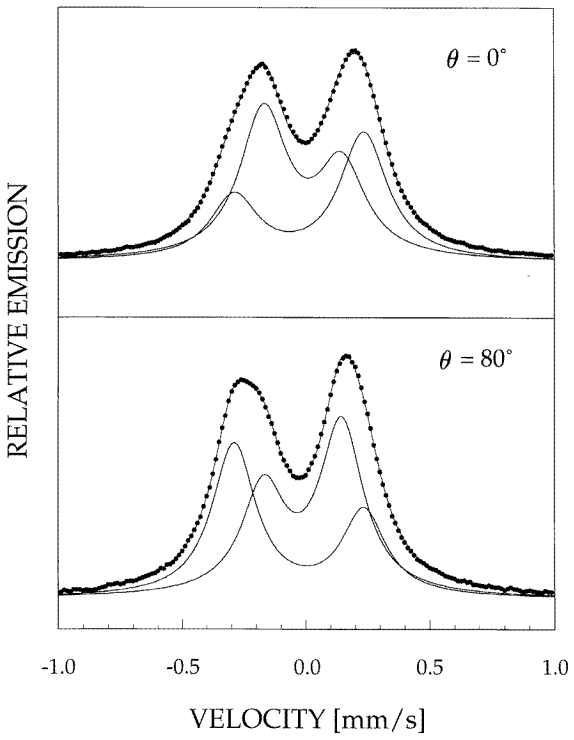

Figure 2. CEMS spectra of β-$FeSi_2$ at different angles θ between the direction of emission of the γ-quantum and the surface normal ($\|c$). The analysis in terms of four lines is indicated.

evidence of an isotropic Lamb–Mössbauer factor for the two sites.

For a single-crystalline sample, the ratio of the intensities of the two transitions $I_{1/2} \rightarrow I_{3/2}$ (I_π) and $I_{1/2} \rightarrow I_{1/2}$ (I_σ) of a quadrupole doublet is angle dependent. If the Lamb–Mössbauer factor is isotropic, one has [22]

$$\frac{I_\pi}{I_\sigma} = \frac{4[(3+\eta^2)/3]^{1/2} + (3\cos^2\Theta - 1 + \eta\sin^2\Theta\cos 2\Phi)}{4[(3+\eta^2)/3]^{1/2} - (3\cos^2\Theta - 1 + \eta\sin^2\Theta\cos 2\Phi)} \tag{1}$$

where Θ and Φ are the polar and azimuthal angles between the direction of emission of the γ-quantum and the main axis of the EFG, and $\eta = (V_{xx} - V_{yy})/V_{zz}$ is the asymmetry parameter. Our coordinate system is the principal axis system in which $|V_{xx}| \leqslant |V_{yy}| \leqslant |V_{zz}|$, and therefore we have $0 \leqslant \eta \leqslant 1$. The quadrupole splitting in velocity units for the $\pm 3/2 \rightarrow \pm 1/2$ transition is

$$\Delta = \frac{eQV_{zz}c}{2E_0}\left(1 + \frac{1}{3}\eta^2\right)^{1/2} \tag{2}$$

where $E_0 = 14.41$ keV is the γ-ray energy, and Q is the nuclear quadrupole moment of the isomeric state of ^{57}Fe. The quadrupole moment is a quantity which is not easily obtained from *ab initio* nuclear models, due to the uncertainty of such models. Earlier estimates have put $Q(^{57}\text{Fe})$ in the range $[-0.19, 0.41]$ b (barns) [23]. More recently, two completely independent methods of determining Q found the concordant result $Q = 0.082$ b [24, 25], but the most recent determination relying on extensive calculations using the highly

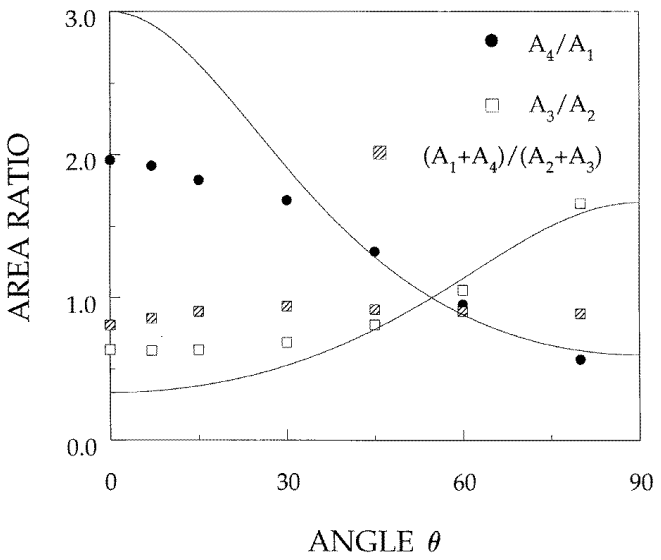

Figure 3. The angular dependence of the ratio of the intensities of the higher- and lower-energy lines for the two quadrupole doublets 1–4, 2–3 and of the population fraction ratio. The solid lines were obtained using equation (1) with $\eta = 0$.

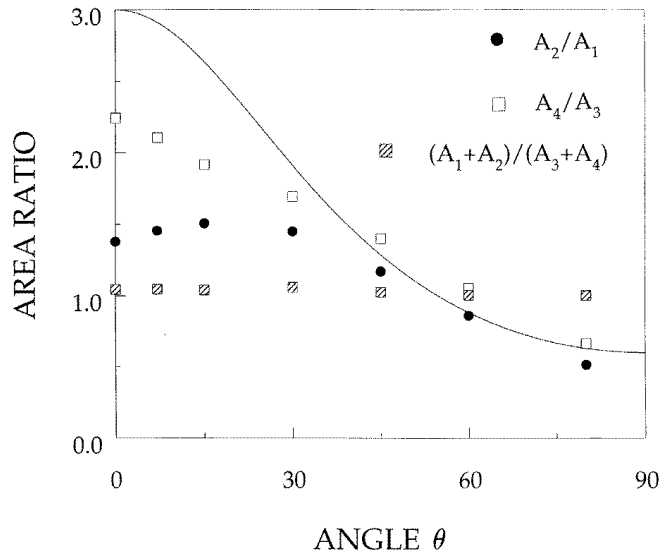

Figure 4. The angular dependence of the ratio of the intensities of the higher- and lower-energy lines for the two quadrupole doublets 1–2, 3–4 and of the population fraction ratio. The solid line was obtained using equation (1) with $\eta = 0$.

accurate full-potential LAPW method revealed a value of $Q = 0.16$ b [26]. These authors compare the electric field gradient calculated for 13 solids, all containing Fe, but with wide variation in bonding nature, with the measured quadrupole splittings, and obtain a

good linear relationship. In the present work we will use the value $Q = 0.16$ b obtained by Dufek *et al*, since our calculations, although not as extensive, seem to confirm their calibration (see the discussion in section 4.2).

The coupling between the lines can be identified from CEMS measurements on the β-$FeSi_2$ sample as function of the angle θ between the γ-direction and the normal ($\parallel$ c) to the sample surface [16]. Equation (1) shows that, due to the presence of rotational domains, the dependence on the azimuthal angle ϕ cannot be observed preventing the experimental determination of the asymmetry parameter η from measurements as function of ϕ [27]. η could be determined from the value of the ratio I_π/I_σ at $\theta = 0$, however different effects, discussed later, affect this ratio. Assuming the coupling 1–4, 2–3 as in figure 2 it can be concluded that the EFG principal axis is oriented along the c axis for both sites which are, however, characterized by opposite signs of the EFG component along this axis. We note that the coupling 1–2, 3–4 (figure 3) results for both sites in a positive value of the EFG component along the principal axis which is approximately along the *c*-axis.

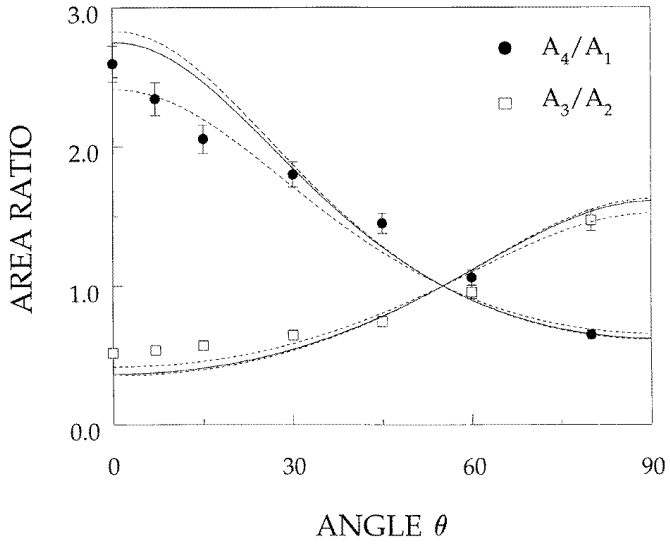

Figure 5. The angular dependence of the ratio of the intensities of the higher- and lower-energy lines for the two quadrupole doublets 1–4, 2–3 corrected for the mixing. The full line is the theoretical prediction for $\eta = 0.4$ integrated because of the geometrical effect. The dotted lines were obtained with the two extreme values, $\eta = 0$ and $\eta = 1$. The error bars have been obtained taking into consideration the results of different measurements and by fitting with parameters within the errors given in table 1.

The theoretical angular dependence of the ratios I_π/I_σ for the two sites in a crystal with $\eta = 0$, an isotropic Lamb–Mössbauer factor, and characterized by rotational domains are shown as solid lines in figure 3. Due to different effects which decrease as the angle θ increases, the experimental data deviate from the theoretical prediction. The geometrical effect due to the finite solid angle related to the sample and source sizes and to the distance between them artificially averages the angular dependence. The effect attenuates the ratio by about 6% at $\theta = 0$ whereas at $\theta = 80^\circ$ it attentuates it by only 3%. In addition the overlapping of the lines in the fitting produces an artificial reduction of the ratio which is $\leqslant$10%. These effects prevent the determination of the asymmetry parameter η from the

Table 1. The Mössbauer parameters of Fe_I and Fe_{II} in β-$FeSi_2$ (δ relative to α-Fe at room temperature). The designation of the Fe_I and Fe_{II} sites is based on the theoretical results.

Site	δ (mm s^{-1})	Γ (mm s^{-1})	Δ (mm s^{-1})	δ_{calc} (mm s^{-1})	V_{zz} (V m^{-2})	η_{calc}	Δ_{calc} (mm s^{-1})
Fe_I	0.076(8)	0.23(2)	+0.525(8)	0.094	$+3.36 \times 10^{21}$	0.36	+0.572
Fe_{II}	0.091(8)	0.23(2)	−0.315(8)	0.109	-1.01×10^{21}	0.41	−0.172

value of the ratio I_π / I_σ at $\theta = 0$. In figure 5 the full lines have been obtained using equation (1) with $\eta = 0.4$ and properly integrated over the source and sample areas (because of the geometrical effect), the experimental data have been corrected for the artificial overlap due to the fitting. Quantitative estimates of the latter corrections have been obtained from the artificial (produced by the fitting due to the overlapping of the lines) angular dependence of the $(A_1 + A_4)/(A_2 + A_3)$ ratio. A deviation in the population of the two sites is in fact conceivable; however, this deviation cannot be angle dependent. Thus the ratio $(A_1 + A_4)/(A_2 + A_3)$ provides a way to estimate the effect of the overlapping. The consideration of all of the effects discussed results in a clearly improved agreement between the expected angular dependence and the experimental data. The remaining deviations may be attributed to various further attenuation effects which are difficult to quantify. We mention for example the presence of randomly oriented small grains, or a texture, as suggested by the RBS minimum channelling yield, and strain. These effects cannot modify the main conclusions; however, additional information (i.e. on the asymmetry parameter) remain inaccessible experimentally.

4. Theory

4.1. The method of the calculations

The electronic structure of β-$FeSi_2$ was calculated with the FP-LMTO method [28] using the local density approximation (LDA) for exchange and correlation effects [29]. This method expands the electron wavefunctions in terms of muffin-tin orbitals [30], which are atom-centred Neumann functions augmented inside muffin-tin spheres by the numerical solution of the radial scalar-relativistic Dirac equation in the self-consistent crystal potential, together with the energy derivative of this solution [31]. This construction has proven very accurate for solid-state calculations [32]. We used three different decay constants for the envelope functions. The basis set used included for each Fe atom 3 orbitals of s character, 3×3 orbitals of p character, 2×5 orbitals of d character and 1×7 orbitals of f character (in short: 3s, 3p, 2d, 1f). Similarly, for the Si atoms the basis functions were chosen as 3s, 3p, 2d. No shape approximation for the crystal potential is invoked. The crystalline charge density is evaluated exactly within muffin-tin spheres, while in the interstitial region an interpolation scheme is used to obtain the charge density [28]. To increase the accuracy of the interpolation scheme, additional 'empty' muffin-tin spheres were included in the open regions of the unit cell. For the evaluation of the Fe electric field gradient it was found important to include the Fe 3p semicore states as band states, which was done in a separate energy panel.

The electric field gradient was calculated using the non-spherical part (in fact, that with

$\ell = 2$) of the crystalline Hartree potential, from which the second-derivative tensor

$$V_{ij} = \frac{\partial^2 V_{H,\ell=2}}{\partial x_i \, \partial x_j}$$

was obtained. Denoting the eigenvalues of V_{ij} by V_{xx}, V_{yy} and V_{zz} with $|V_{xx}| \leqslant |V_{yy}| \leqslant |V_{zz}|$, the electric field gradient per definition is equal to V_{zz}, while the asymmetry parameter is

$$\eta = \frac{V_{xx} - V_{yy}}{V_{zz}}$$

which lies in the range $[0, 1]$ (since $V_{xx} + V_{yy} + V_{zz} = 0$).

Table 2. Representative atomic coordinates in the β-$FeSi_2$ unit cell; cf. equation (3) (from reference [10]). The other atomic positions follow from the $Cmca$ (D_{2h}^{18}) group symmetry.

	U	*V*	*W*
Fe_I	0.0	0.0	0.214 65
Fe_{II}	0.308 61	0.315 04	0.0
Si_I	0.274 65	0.051 20	0.128 23
Si_{II}	0.044 99	0.226 08	0.372 71

The crystal structure of β-$FeSi_2$ is base-centred orthorhombic with eight formula units in the primitive cell. The positions of the atoms are characterized by a number of structural parameters, which have been determined experimentally [10]. Table 2 summarizes this information. The representative Fe and Si positions are denoted by

$$\boldsymbol{R}_i = U_i \boldsymbol{a} + V_i \boldsymbol{b} + W_i \boldsymbol{c} \tag{3}$$

with i = I, II, III, IV, for Fe_I, Fe_{II}, Si_I and Si_{II}, respectively. The two inequivalent Fe sites are each surrounded by their distorted cubes of eight Si atoms. The calculations presented here used the experimental structural parameters. To determine the sensitivity of the electric field gradient we also report calculations with slightly different parameters. The calculations used 21 k-points in the irreducible eighth of the Brillouin zone (and for convergence tests sometimes 52 and 105 k-points were used), and the tetrahedron method was used to construct the charge density [31].

4.2. Results

The electric field gradients (V_{zz}) of Fe_I and Fe_{II} are calculated to be 3.36×10^{21} V m^{-2} and -1.01×10^{21} V m^{-2}, respectively. See table 1. In both cases the corresponding direction of maximal variation of the Hartree potential coincides with the crystallographic c-axis. The asymmetry parameter is significant and similar, 0.36 and 0.41, for the two sites. The difference in sign of the electric field gradient implies that the electrostatic potential increases along the c-axis but decreases along both the a-axis and the b-axis for the Fe_I site, while for the Fe_{II} the electrostatic potential decreases along the c-direction but increases along the a-direction and b-direction.

We have tested the sensitivity of the electric field gradient to the structural parameters of β-$FeSi_2$. The variation of the calculated Fe electric field gradients with the parameters (U_i, V_i, W_i) (see equation (3) and table 2) are quoted in tables 3 and 4. Also quoted is the volume dependence of the electric field gradient, i.e., the variation due to a rigid scaling of all crystal distances.

Table 3. Calculated relative changes of the electric field gradients in β-FeSi$_2$ due to changes in volume (Ω) and internal coordinates of the Fe atoms; cf. table 2 and equation (3).

	$\frac{\mathrm{d}\ln\lvert V_{zz}\rvert}{\mathrm{d}\ln\Omega}$	$\frac{\mathrm{d}\ln\lvert V_{zz}\rvert}{(c/a)\ \mathrm{d}W_{\mathrm{I}}}$	$\frac{\mathrm{d}\ln\lvert V_{zz}\rvert}{\mathrm{d}U_{\mathrm{II}}}$	$\frac{\mathrm{d}\ln\lvert V_{zz}\rvert}{(b/a)\ \mathrm{d}V_{\mathrm{II}}}$
Fe$_{\mathrm{I}}$	−1.6	−13.4	+1.5	−1.8
Fe$_{\mathrm{II}}$	+3.6	−38	+35	+42

Table 4. Calculated relative changes of the electric field gradients in β-FeSi$_2$ due to changes in internal coordinates of the Si atoms; cf. table 2 and equation (3).

	$\frac{\mathrm{d}\ln\lvert V_{zz}\rvert}{\mathrm{d}U_{\mathrm{III}}}$	$\frac{\mathrm{d}\ln\lvert V_{zz}\rvert}{(b/a)\ \mathrm{d}V_{\mathrm{III}}}$	$\frac{\mathrm{d}\ln\lvert V_{zz}\rvert}{(c/a)\ \mathrm{d}W_{\mathrm{III}}}$	$\frac{\mathrm{d}\ln\lvert V_{zz}\rvert}{\mathrm{d}U_{\mathrm{IV}}}$	$\frac{\mathrm{d}\ln\lvert V_{zz}\rvert}{(b/a)\ \mathrm{d}V_{\mathrm{IV}}}$	$\frac{\mathrm{d}\ln\lvert V_{zz}\rvert}{(c/a)\ \mathrm{d}W_{\mathrm{IV}}}$
Fe$_{\mathrm{I}}$	+12.9	−7.7	−0.5	−6.9	−4.8	+10.6
Fe$_{\mathrm{II}}$	+38	−37	−81	−16.7	−21	+77

The electric field gradient of the Fe$_{\mathrm{II}}$ site is very sensitive to structural changes, while that of the Fe$_{\mathrm{I}}$ site is more robust. Part of this variation is due to the fact that the electric field gradient on the Fe$_{\mathrm{II}}$ site is smaller in absolute size. Thus, for the rigid volume scaling and for the movement of the Fe$_{\mathrm{I}}$ atom, the relative variation of the field gradient is approximately three times larger for the Fe$_{\mathrm{II}}$ site than for the Fe$_{\mathrm{I}}$ site. For example, shifting the position of Fe$_{\mathrm{I}}$ by $0.01a$ along the c-axis diminishes the electric field gradient on the Fe$_{\mathrm{I}}$ site by 13.4% (to 2.90×10^{21} V m^{-2}) and the electric field gradient on the Fe$_{\mathrm{II}}$ site by 38% (to -0.62×10^{21} V m^{-2}), i.e., the absolute changes are about equal. On the other hand, for movement of the Fe$_{\mathrm{II}}$ position the electric field gradient on the Fe$_{\mathrm{I}}$ site is relatively unaffected, while the electric field gradient on the Fe$_{\mathrm{II}}$ site changes significantly, again by of the order of 40% for displacements of size $0.01a$ along the a-direction or b-direction. Similar results have also been found for movements of the Si atoms by small amounts within the unit cell. We conclude that the electric field gradient on the Fe$_{\mathrm{II}}$ site is a more sensitive quantity to calculate than the electric field gradient on the Fe$_{\mathrm{I}}$ site. In the light of this, the agreement obtained in table 1 with the experimental Mössbauer quadrupole splitting must be considered satisfactory.

Table 5. Electric field gradients in FeS$_2$ (pyrite and marcasite structures) and ϵ-FeSi. The results of the present work are compared to the FP-LAPW calculations of Dufek *et al* (reference [26]) and to experimental data (as collected in reference [26]). The sign of the electric field gradients has not been determined experimentally. The units are 10^{21} V m^{-2}.

	Dufek *et al*	This work	Experiment
FeS$_2$ (pyrite)	−3.47	−3.17	3.66
FeS$_2$ (marcasite)	−3.36	−3.27	3.00
ϵ-FeSi	+4.92	+4.32	4.45

We stress that the value of $Q = 0.16$ b as obtained by Dufek *et al* [26] was used to convert to the experimental units (mm s^{-1}), and that the smaller value of $Q = 0.082$ b would not give such a good agreement. We have in table 5 for a few compounds (FeS$_2$ and ϵ-FeSi) compared the electric field gradient as calculated in the present approach with the

results of Dufek *et al*. The agreement with experiment (again converting using the larger value of Q) is good and comparable to that between the theoretical studies. The details of the calculational schemes are quite different, although both studies rely on present-day state-of-the-art *ab initio* solid-state electronic structure methods, notably the full-potential LAPW used by Dufek *et al* versus the full-potential LMTO method in the present work. Dufek *et al* additionally include some localized basis functions to achieve higher accuracy, which we have not found necessary in the present scheme. Finally, Dufek *et al* used the generalized gradient approximation (GGA) for exchange and correlation effects, where we used the local density approximation. In their extensive study, Dufek *et al* found only minor differences between the electric field gradients calculated with the GGA and the LDA, except for in those important cases where the LDA gives a qualitatively wrong ground state while GGA gives the correct one. This happens for example in FeF_2, but not in ϵ-FeSi, and therefore most probably not in β-$FeSi_2$ either.

To determine the electron contact density of the Fe_I and Fe_{II} sites in β-$FeSi_2$, the nucleus was modelled by a uniformly charged sphere of radius $R = 1.2\,A^{1/3}$ fm, where $A = 57$ is the mass number of the Fe nucleus. The contact density was obtained as an average over the nuclear volume. All core states were calculated self-consistently in the crystalline environment.

The electron contact density was found to be practically identical at the two Fe sites, being higher at the Fe_I site than at the Fe_{II} site by 0.07 au, which corresponds to an isomer shift difference of 0.014 mm s^{-1} (using the Fe isomer shift calibration of reference [18]). This is in excellent agreement with the experimental difference of 0.015 mm s^{-1} for the 1–4, 2–3 coupling. In the previous calculations based on the atomic-sphere approximation the electron contact density of Fe_I was found to be higher than that of Fe_{II} by 0.17 au [16]. Thus, as regards the isomer shift, the ASA- and the FP-LMTO results, agree well with the experiments if the 1–4, 2–3 coupling is used. In contrast, the alternative 1–2, 3–4 coupling would imply an isomer shift difference of 0.42 mm s^{-1}, corresponding to a difference in contact density of close to 2 au, which is clearly at variance with both theoretical results. The small and positive EFG values resulting from this coupling are also in disagreement with the theoretical results. By comparing two LMTO calculations with slightly different parameters we estimate the uncertainty on the calculated isomer shift to be 0.01 mm s^{-1}. The calculations reveal a quite similar electronic structure of the Fe_I and Fe_{II}. Although the 'charge transfers' cannot be unambiguously defined, *differences* between the charges accumulated near the Fe_I and Fe_{II} sites can be estimated to be $q_I - q_{II} \approx 0.1$ electrons by integrating over a sphere (with the radius taken to be 2.5 au). The extra charge on Fe_I has both s and pd character, with the direct increase of the electron contact density due to increased s-electron occupancy dominating over the decrease due to screening of the s-partial-wave states and core states by enhanced non-s charge.

Finally, we would like to comment on the signs and values of the EFG for the two inequivalent Fe sites. Calculations of the EFG within the point charge model [13, 14] give a negative sign on both sites and a ratio of $EFG_I/EFG_{II} = 0.83$. However, when the bonding has a significant covalent component, as in β-$FeSi_2$, the local polarization of the electron cloud around the Fe nucleus is not merely given by an antishielding factor [33] times the point lattice contribution. In fact, we have repeated the point charge calculation using the electronic charges as found in our self-consistent LMTO calculation rather than some perfect ionic charges. This leads to a muffin-tin model of the charge distribution in the solid with positive point charges in a homogeneous compensating negative background. This calculation also gives almost identical values of the EFG at the two Fe sites: $+0.50 \times 10^{21}$ V m^{-2} and $+0.54 \times 10^{21}$ V m^{-2}, at the Fe_I and Fe_{II} sites (no antishielding factor included).

These numbers are far from the total self-consistent values of $+3.36 \times 10^{21}$ V m^{-2} and -1.01×10^{21} V m^{-2} (table 1). Moreover, the asymmetry parameter is close to zero and the directions of maximal field gradient variation are within the *ab*-plane, rather than along the crystallographic *c*-axis, as in the full calculation. We conclude that the point charge model is totally inadequate for the computation of the EFG in β-FeSi$_2$.

5. Conclusions

The two Fe sites in β-FeSi$_2$ have been investigated by CEMS. From the angular dependence of the line intensities the correct coupling has been determined. The two Fe sites in β-FeSi$_2$ have approximately identical isomer shifts, but the electric field gradients are very different both in magnitude and in sign. Full-potential LMTO calculations of the isomer shift and quadrupole interaction at the two sites were found to be in good agreement with the experimental findings. The Fe$_{\rm I}$ atom was found to have a positive electric field gradient, while the Fe$_{\rm II}$ atom has a negative electric field gradient of size approximately a third of that of Fe$_{\rm I}$. In both cases the principal axis is along the crystalline *c*-axis. The calculated quadrupole splittings are in good agreement with the experimental data provided that the recently obtained value of $Q = 0.16$ b for the ^{57}Fe nuclear quadrupole moment is adopted. Due to different effects the experimental determination of the asymmetry parameter remains inaccessible. The present work demonstrates the usefulness of combining advanced Mössbauer experimental techniques with state-of-the-art electronic structure schemes in analysing Fe-based materials.

Acknowledgments

It is a pleasure to thank C Schwarz who performed the RBS measurement. This work has been supported by the Danish Accelerator Physics and Natural Science Research Councils (grant No 11-0694-1) as well as the Commission of the European Union, contract No CI1*CT92-0086.

References

[1] Bost M C and Mahan J E 1985 *J. Appl. Phys.* **58** 2696
[2] Dimitriadis C A, Werner J H, Logothetidis S, Stutzmann M, Weber J and Nesper R 1990 *J. Appl. Phys.* **68** 1726
[3] Christensen N E 1990 *Phys. Rev.* B **42** 7148
[4] Wang L, Qin L, Zheng Y, Shen W, Chen X, Lin X, Lin C and Zou S 1994 *Appl. Phys. Lett.* **65** 3105
[5] Eppenga R 1990 *J. Appl. Phys.* **68** 3027
[6] Miglio L and Malegori G 1995 *Phys. Rev.* B **52** 1448
[7] Giannini C, Lagomarsino S, Scarinci F and Castrucci P 1992 *Phys. Rev.* B **45** 8822
[8] Olk C H, Yalisove S M and Doll G L 1995 *Phys. Rev.* B **52** 1692
[9] Kubaschewski O 1982 *Iron-Binary Phase Diagrams* (Berlin: Springer)
[10] Dusausoy P Y, Protas J, Wandji R and Roques B 1971 *Acta Crystallogr.* B **27** 1209
[11] Geib K M, Mahan J E, Long R G and Nathan M 1991 *J. Appl. Phys.* **70** 1730
[12] von Känel H, Kafader U, Sutter P, Onda N, Sirringhaus H, Müller E, Kroll U, Schwarz C and Goncalves-Conto S 1994 *Mater. Res. Soc. Symp. Proc.* **320** 73
[13] Wandji R, Le Corre C, Genin J M and Roques B 1971 *Phys. Status Solidi* b **45** K123
[14] Blaauw C, van der Woude F and Sawatzky G A 1973 *J. Phys. C: Solid State Phys.* **6** 2371
[15] Helgason Ö and Sigfüsson T I 1989 *Hyperfine Interact.* **45** 415
[16] Fanciulli M, Rosenblad C, Weyer G, Svane A, Christensen N E and von Känel H 1995 *Phys. Rev. Lett.* **75** 1642

[17] Christensen N E, Svane A, Fanciulli M, Weyer G, Methfessel M and Rodriguez C O 1996 *Bull. Am. Phys. Soc.* **41** 788
[18] Eriksson O and Svane A 1989 *J. Phys.: Condens. Matter* **1** 1589
[19] Weyer G 1976 *Mössbauer Eff. Methodol.* **10** 301
[20] Afanas'ev A M and Tsymbal E Yu 1990 *Hyperfine Interact.* **61** 325
[21] Goldanskii V I and Herber R H 1968 *Chemical Applications of Mössbauer Spectroscopy* (London: Academic)
[22] Zory P 1965 *Phys. Rev.* A **140** 1401
[23] Greenwood N N and Gibb T C 1971 *Mössbauer Spectroscopy* (London: Chapman and Hall)
[24] Duff K J, Mishra K C and Das T P 1981 *Phys. Rev. Lett.* **46** 1611
[25] Vajda S, Sprouse G D, Rafailovich M H and Noe J W 1981 *Phys. Rev. Lett.* **47** 1230
[26] Dufek P, Blaha P and Schwarz K 1995 *Phys. Rev. Lett.* **75** 3545
[27] In reference [16] we erroneously estimated an upper limit of the asymmetry parameter on the basis of the observed azimuthal isotropy.
[28] Methfessel M 1988 *Phys. Rev.* B **38** 1537
Methfessel M, Rodriguez C O and Andersen O K 1989 *Phys. Rev.* B **40** 2009
[29] Jones R O and Gunnarsson O 1989 *Rev. Mod. Phys.* **61** 689
[30] Andersen O K 1975 *Phys. Rev.* B **12** 3060
[31] See, e.g.,
Skriver H L 1984 *The LMTO Method* (Berlin: Springer)
[32] Andersen O K, Jepsen O and Glötzel O 1985 *Canonical Description of the Band Structures of Metals; Proc. Int. School of Physics (Varenna, 1985)* course LXXXIX, ed F Bassani, F Fumi and M P Tosi (Amsterdam: North-Holland) p 59
[33] Sternheimer R M 1951 *Phys. Rev.* **84** 244
Sternheimer R M 1952 *Phys. Rev.* **86** 316
Sternheimer R M 1954 *Phys. Rev.* **95** 736